Scaling behaviour of rf surface resistance in oxygen deficient single-domain YBCO

2000 Supercond. Sci. Technol. 13 902

(http://iopscience.iop.org/0953-2048/13/6/356)

Supercond. Sci. Technol. **13** (2000) 902–907. Printed in the UK PII: S0953-2048(00)11616-1

Scaling behaviour of rf surface resistance in oxygen deficient single-domain YBCO

D Qu†, Donglu Shi†, Altan Ferendeci‡, David Mast§, H A Blackstead‖ and I Maartense¶

† Department of Materials Science & Engineering, University of Cincinnati, Cincinnati, OH 45220, USA
‡ Department of Electrical & Computer Engineering, & Computer Science, University of Cincinnati, Cincinnati, OH 45220, USA
§ Department of Physics, University of Cincinnati, Cincinnati, OH 45220, USA
‖ Physics Department, University of Notre Dame, Notre Dame, IN 46556, USA
¶ MLPO, AFRL, Wright-Patterson AFB, OH 45433, USA

Received 4 February 2000

Abstract. To develop high-quality rf components for wireless telecommunications, we have processed single-domain YBCO of various dimensions and geometry for the device applications including high-Q resonators and filters. In this development, a critical parameter, the surface resistance, R_s, of single-domain YBCO has been measured in wide ranges of temperature and magnetic field. We have found that the Pippard model can best describe the well oxygenated crystal, indicating the high-quality of single-domain YBCO. However, such scaling breaks down when the oxygen structural disorders are introduced into the sample. A fundamentally different scaling behaviour is observed, which is closely related to the structural defects of oxygen. We report such a behaviour and discuss the possible underlying mechanism.

1. Introduction

Low surface resistance, R_s, is a key property of conductors used in rf device applications. For a normal conductor such as copper, the surface resistance is of the order of 0.01 Ω at a frequency of 2 GHz [1, 2]. The surface resistance is many orders of magnitude below this at the same frequency range in well textured YBCO, making this HTS material an attractive candidate for rf components [4–17]. To achieve low surface resistance, the current approaches in processing HTSs are thin-film technologies, which can produce epitaxially grown films with low surface resistance [4–17]. In this work, we have utilized a single-crystal-like, single-domain YBCO as an alternative but equally effective material. With today's technology, the single-domain YBCO can be readily processed at dimensions up to 60 mm in a diameter. Such a large volume allows a three-dimensional architecture of the rf component, such as tunable filters. The advantages also include easy manipulation of the geometry, large cross sectional area, and great freedom in dimensionality control. These advantages provide unique opportunities in rf component engineering and device design.

There have been limited data on the surface resistance of single-domain YBCO. Our preliminary experiments have shown that the surface resistance of the single-domain YBCO measured at 77 K and 0.8 GHz has reached 0.05 mΩ, indicating an extremely low value comparable to those of thin films. In addition, our previous work has also shown respectable Q values up to 10^4, measured from a substrateless cavity resonator measured at 18 GHz. However, there have been no previous studies on the effects of structural defects on R_s in single-domain YBCO. In this paper, we present experimental data on the surface resistance of a series of single-domain samples that have been annealed at different temperatures. We show that, due to oxygen disorder, the field dependence of R_s in a wide range of temperatures exhibits a unique scaling behaviour. We discuss the possible underlying mechanism.

2. Experimental details

2.1. Sample preparation

The single-domain materials used in this study were processed by the seeded melt growth (SMG) method which has been previously reported [6–8]. The samples for this work were sectioned from a large single-domain material processed by the SMG method.

In order to avoid the influence of run-to-run processing variations on the microwave properties, all the small cubic samples to be tested were prepared from one large single domain of YBCO. A well polished single-domain YBCO

0953-2048/00/060902+06$30.00

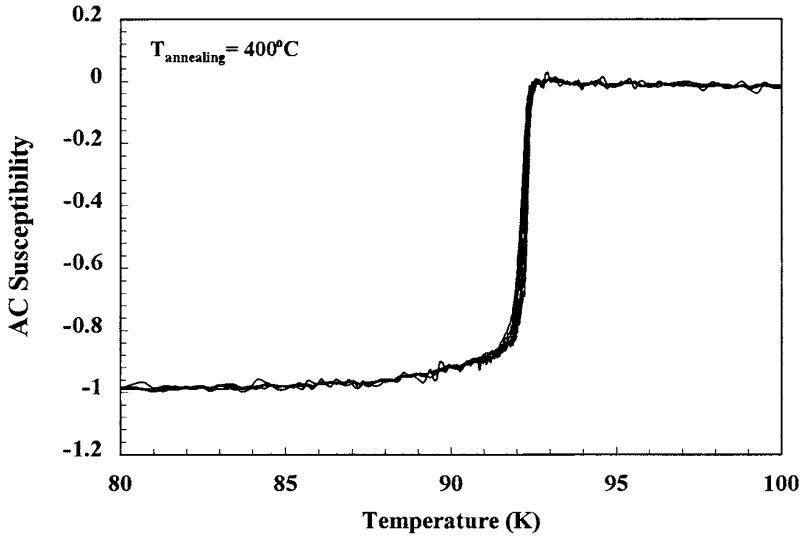

Figure 1. Ac susceptibility versus temperature for the 400 °C-annealed sample at fields of, from left to right, 2.2, 1.5, 1.0, 0.5, 0.25 and 0.1 Oe.

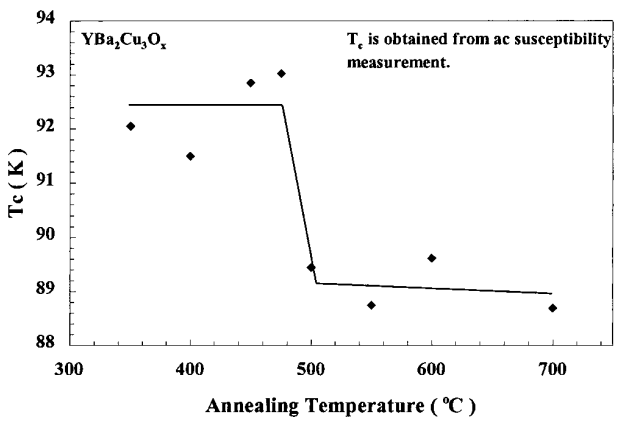

Figure 2. T_c onset values versus annealing temperature for several single-domain YBCO samples with dimensions $1 \times 1 \times 0.5$ mm^3.

Table 1. The equilibrium oxygen content (x) in $YBa_2Cu_3O_x$ under different annealing temperatures with oxygen flow [9].

T_{anneal} (°C)	350	400	450	500	550
x	6.86	6.85	6.83	6.80	6.75

was cut into small cubic samples with dimensions of $1 \times 1 \times 0.5$ mm^3 and these samples were annealed in flowing oxygen at different temperatures (350 °C, 400 °C, 450 °C, 500 °C, 550 °C) for 48 h.

The oxygen ordering has been found to be an important structural factor that dictates many superconducting parameters. Earlier neutron diffraction work has established a relation between the equilibrium oxygen content and the critical temperature for YBCO at different atmospheric conditions [9–13]. In table 1, we list the corresponding equilibrium oxygen content at these temperatures based on the neutron data. According to these results, we have carried out annealing experiments at 350 °C, 400 °C, 450 °C, 500 °C and 550 °C. Presumably, annealing for fixed times at these temperatures would produce different oxygen orderings in the samples.

The annealing was done using a horizontal tube furnace. The sample was placed on an alumina substrate. The annealing was carried out individually for each sample group (i.e. for each temperature, we annealed multiple samples for repeated measurements). During the annealing, the sample was heated at a rate of 100 °C h^{-1} up to the annealing temperature, held for 48 h, then the sample was quenched to room temperature in air.

3. Surface resistance measurement

After annealing, the cubic samples were ready for the surface resistance measurement. Surface resistance was measured in a rectangular resonator cavity (TE_{101} mode). The sample was placed on the bottom of the cavity. Power was coupled into the cavity through an iris with a coupling coefficient that was made variable by using a Gordon coupler, which provided the impedance matching and facilitated operation at optimal sensitivity [14]. In the measurement, the applied magnetic field could be rotated to be parallel or perpendicular to the rf current. As rf dissipation changed in the sample, this changed the losses in the cavity, and the cavity's quality factor (Q value). In turn, this changed the impedance match of the waveguide to the cavity and the power reflected from the cavity. Changes in the reflected power were detected as changes in the dc diode voltage. Temperature-induced changes in the cavity were smaller than those of the sample. The background changes were determined with empty cavity measurements and subtracted from the signal to yield the superconducting response. In the normal state, the surface resistance for bulk sample is given by $R_s = (\mu_0 \omega \rho(T)/2)^{1/2}$. At low temperature, the superconducting surface resistance approaches zero. The application of magnetic field in excess of B_{c1} leads to the formation of vortices, which have a normal core. The rf current density interacts with the vortices, inducing a small vibration amplitude, which is typically less than an angstrom in amplitude. This small amplitude motion of the normal core causes dissipation, which is readily detected. The resulting surface resistance varies roughly as

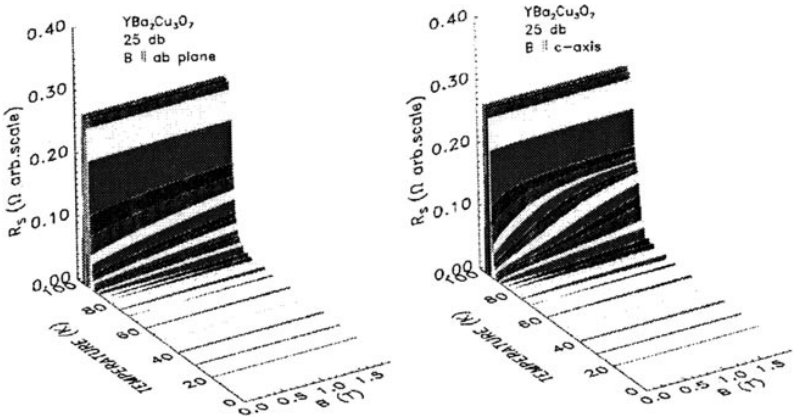

Figure 3. Three-dimensional plots of R_s as a function of the temperature and magnetic field: (a) the field is parallel to the ab-plane, (b) the field is parallel to the c-axis.

$B^{1/2}$, providing a nearly unique signature characteristic of dissipation in the superconducting state.

4. Results and discussion

To characterize the bulk properties of these annealed samples, we conducted ac susceptibility measurements at different applied fields. Figure 1 shows the ac susceptibility versus temperature at different ac magnetic fields for the full-oxygenated YBCO sample (annealed at 400 °C). As can be seen, the sample exhibits an extremely sharp superconducting transition comparable to the behaviour of the best single crystals of YBCO reported. These data indicate a highly single-crystal-like nature in the single-domain YBCO. Figure 2 shows the T_c onset values from the ac susceptibility measurements plotted against annealing temperature. From this figure, we have observed a plateau region. Interestingly, the lower plateau occurs at a much higher transition temperature of 89 K than the previous data on the ceramic polycrystalline sample, which showed a plateau at 60 K. We note that the ac susceptibility data reflect a bulk behaviour of the material.

However, the surface resistance measurements in this work have shown quite different behaviours compared with the ac susceptibility measurements. The measurements of surface resistance (R_s) have been carried out under different applied dc magnetic fields. In figure 3, we show R_s of the 400 °C-annealed sample plotted as a function of temperature and magnetic field (B) for fields applied parallel and normal to the c-axis of the crystal. As can be seen from this figure, the sample exhibits sharp transitions for both orientations at low fields but, however, shows quite different field dependences up to 1.5 T. For B parallel to the ab-plane configuration, the field dependence exhibits a linear behaviour even for the high field region, indicating a strongly-coupled superconducting surface. As the field is applied normal to the ab-plane (B parallel to the c-axis), the field dependence shows nonlinear behaviour, although the specific dependence is under investigation. Nonetheless, from these data we can observe an interesting surface behaviour for different orientations of the magnetic field. It appears that a field parallel to the ab-plane produces a much lower R_s, especially in the high field region, while the field normal to the ab-plane tends to raise R_s considerably, even at low fields up to 0.5 T, as shown in figure 3.

For better analysis of the experimental data, we plot the surface resistance difference, $\Delta R_s = R_s(B) - R_s(B = 0)$. In this way, we can see the R_s transition from a two-dimensional plot. The results of ΔR_s of some typical samples are plotted in figure 4 as a function of temperature for different magnetic fields. From this figure, one can clearly see the broadening effects due to oxygen ordering. The samples annealed at 400 °C are fully oxygenated and therefore exhibit the sharpest transitions. However, as the annealing temperature is increased to 550 °C, considerably broadening is evident, as shown in figure 4. This behaviour is clearly associated with the oxygen disorder in the unit cell, although the exact mechanics is not understood at this point. At 350 °C, the equilibrium concentration of oxygen is, in fact, higher than that of 400 °C; however, the broadening in ΔR_s is even more severe. We believe that this can be attributed to the slow oxygen diffusion at such a low annealing temperature. A prolonged anneal may further oxygenate the sample and suppress the peak broadening.

To further analyse the data we have normalized ΔR_s, which allows us to see the scaling behaviour in the magnetic field. Figure 5 shows the normalized R_s versus temperature for the 400 °C-annealed sample for both $B \| c$ and $B \| ab$. As can be seen in this figure, normalization has resulted in quite similar scaling at all magnetic fields for both configurations. This suggests a common operating mechanism for the temperature dependence of the surface resistance. According to Pippard [15], the temperature dependence of R_s can be expressed as

$$R_s = f(\omega)t^{\alpha}(1 - t^2)/(1 - t^4)^2$$

where $t = T/T_c$. The fitting of these curves in the superconducting state has resulted in a power-law behaviour as shown in figure 6 for both $B \| c$ and $B \| ab$ with $\alpha = 2$. As can be seen in this figure, the Pippard model, which describes a single crystal of a type II superconductor, has fitted the single-domain YBCO quite well. The excellent agreement between the model and the experimental data indicates that (1) an exceptionally high-quality single-crystal-like superconductor and (2) the basic microwave behaviour

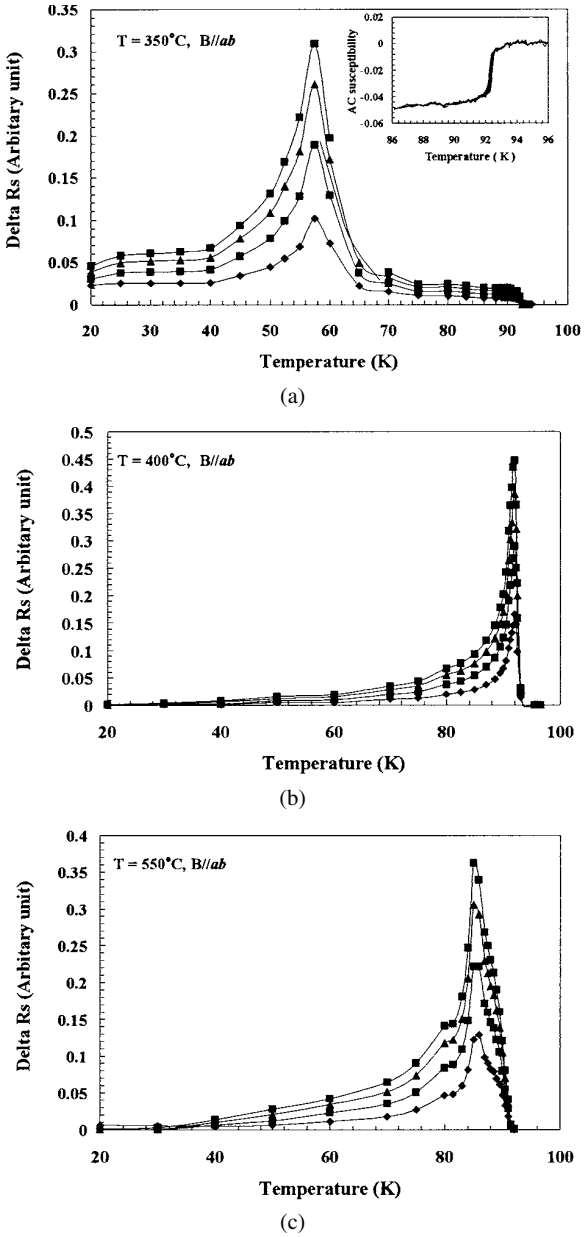

Figure 4. ΔR_s versus temperature for the samples annealed at temperatures indicated. The applied field, from left to right, is 1.9, 1.5, 1.0 and 0.5 T.

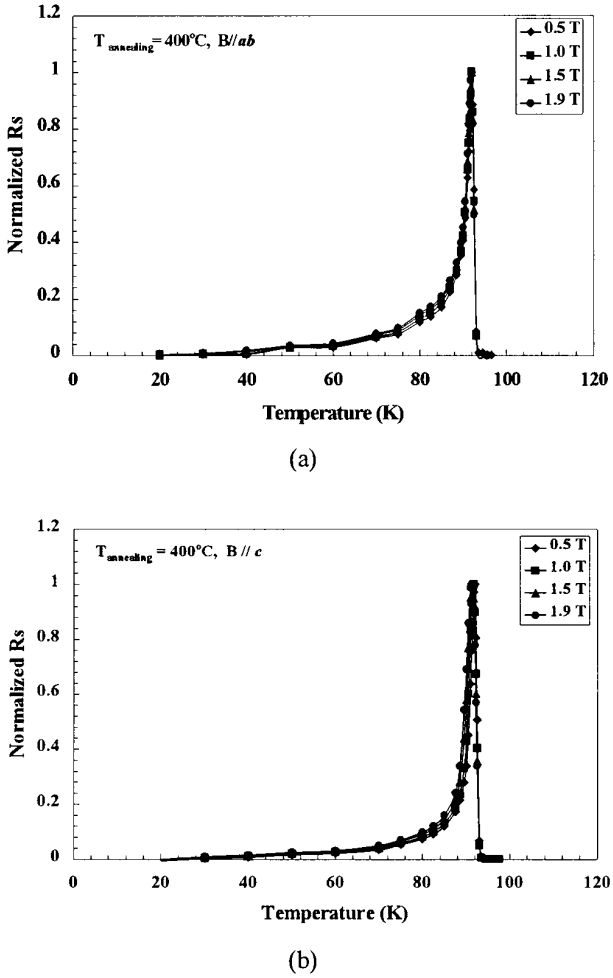

Figure 5. Normalized R_s versus temperature for the sample annealed at 400 °C: (a) the fields are parallel to the *ab*-plane, (b) the fields are parallel to the *c*-axis.

observed in the single-domain YBCO is similar to those of conventional type II superconductors. However, a physical model will have to be established to further explain the loss mechanisms in the single-domain YBCO, including the interaction between vortices and rf currents. This modelling work is currently under investigation.

For the oxygen deficient samples annealed at 350 °C and 550 °C, we have observed fundamentally different scaling behaviours as shown in figures 7 and 8. We note here that the 350 °C-annealed sample exhibits reasonably sharp superconducting transitions in the ac susceptibility measurements as shown in the inset of figure 4(a). This difference indicates that the bulk oxygenation can be quite sufficient at 350 °C while the surface oxygen of the sample has been depleted to a certain degree, resulting in a decreased rf transition near 60 K. As can be seen in figure 7, the rf transitions occurred near 60 K at all applied fields and the transition widths are quite broadened for both configurations (see figures 7(a) and 7(b)). In particular, when the applied field is parallel to the *c*-axis, normalization has resulted in the significantly different scaling behaviours at various magnetic fields. In other words, under each field the physical processes may differ from one another, indicating a considerable disordered structure in the sample. The 550 °C-annealed sample exhibited similar behaviours as shown in figure 8. Due to a relatively lower oxygen concentration at 550 °C, the transition has decreased to near 80 K with a considerable broad transition width at each field. For the $B \| c$ configuration (see figure 8(b)), not only have we observed different scaling laws at each field, but also a second peak just below 80 K. This small peak could suggest a different superconducting phase as a result of oxygen deficiency. However, as shown in figure 8(a) for $B \| ab$, this second peak appears to be smaller, indicating a less pronounced effect.

As evidenced in figures 7 and 8, the broadening effects are more pronounced for $B \parallel c$. As introduced above, the surface resistance was measured in a rectangular resonator cavity (TE_{101} mode). In the measurement, the applied

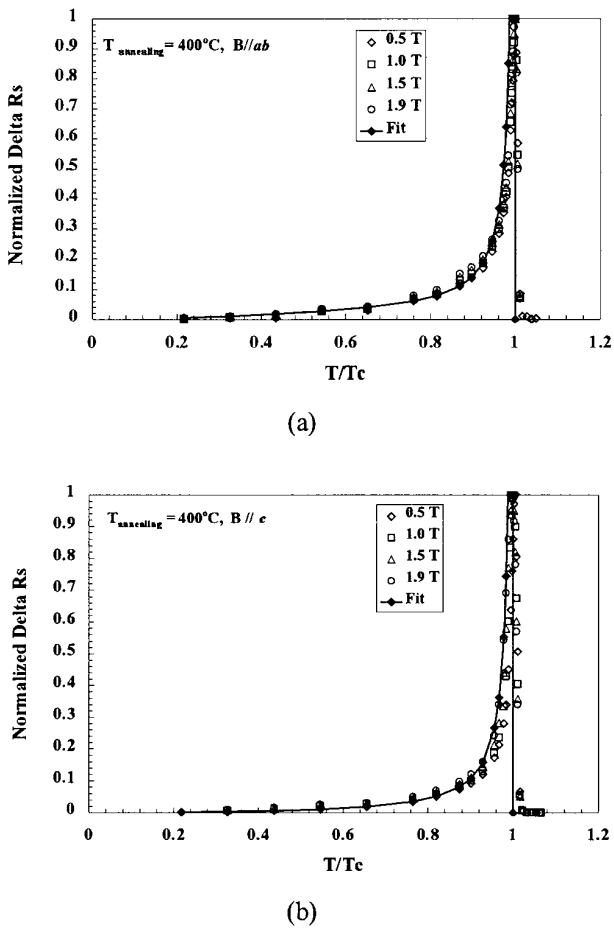

Figure 6. The normalized ΔR_s versus temperature for the 400 °C-annealed sample. The full curve is the Pippard model fit to the data with $\alpha = 2$: (a) the fields are parallel to the *ab*-plane, (b) the fields are parallel to the *c*-axis.

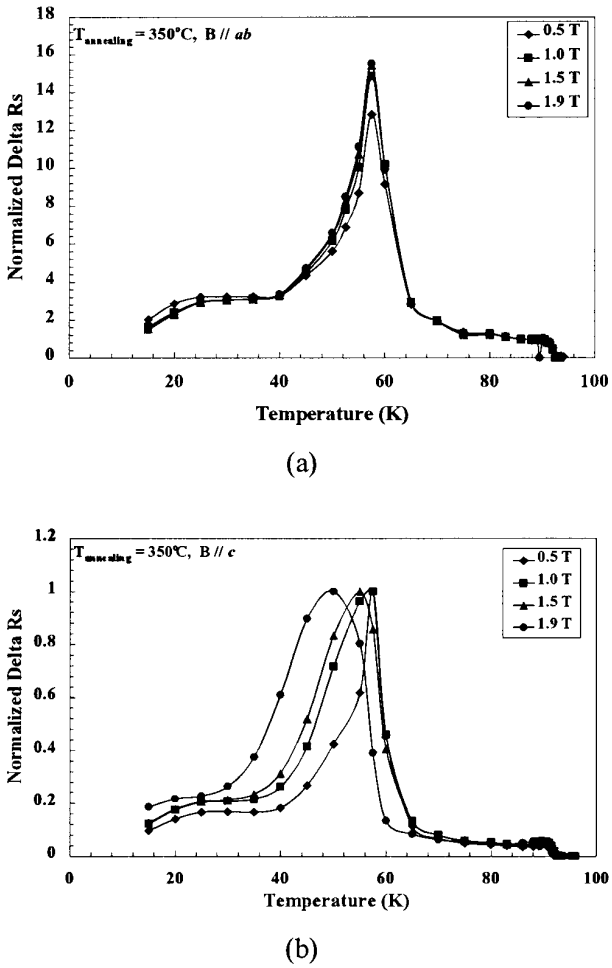

Figure 7. Normalized ΔR_s versus temperature for the sample annealed at 350 °C: (a) the fields are parallel to the *ab*-plane, (b) the fields are parallel to the *c*-axis.

magnetic field could be rotated to be parallel or perpendicular to the rf current. In the oxygen deficient samples, rf dissipation is affected by the oxygen structural defects, particularly in the magnetic field. In the normal state, the surface resistance for the bulk sample is given by $R_s = (\mu_0 \omega \rho(T)/2)^{1/2}$. At low temperature, the superconducting surface resistance approaches zero. As the magnetic field exceeds B_{c1}, the vortices are formed in the sample matrix. These vortices are generally parallel to the applied field. The rf current density will interact with these vortices, creating a small vibration amplitude, typically less than an angstrom in amplitude. This small amplitude motion of the normal core causes dissipation, which is readily detected. As the applied field is parallel to *ab*-planes, the vortices are strongly pinned by these planes. In this configuration, the motion of the normal cores becomes rather difficult resulting in a smaller dissipation. However, the situation is changed drastically when the field is applied normal to the *ab*-planes. The normal cores are weakly pinned in this configuration, and their interaction with rf currents will drive the vortices into motion, and in turn cause dissipation. Therefore, in figures 7 and 8, we observed more pronounced broadening effects. Furthermore, the oxygen structural defects can form weak superconducting regions in the sample. Not only is the order parameter suppressed in these regions, but the vortex pinning is also weakened. As a consequence, T_c has decreased considerably to 60 K and 80 K for the 350 °C-annealed and the 550 °C-annealed samples, respectively. Note that the rf measurements can only detect losses on the sample surface approximately 1 μm deep. This is essentially different from the ac susceptibility measurement that determines the losses due to vortex motion in and out of the bulk matrix of the sample. Therefore, although the inset in figure 4(a) shows quite sharp T_c for the 350 °C-annealed sample, the R_s behaviour is entirely different, as can be seen in figure 7. This sharp contrast indicates a severe surface oxygen depletion while the bulk oxygen is sufficiently high. Further analysis of the oxygen distribution in the sample matrix is under investigation.

5. Conclusion

By measuring R_s in a wide range of magnetic field, we have observed different scaling behaviours due to oxygen disorder in the sample. For a well oxygenated sample annealed at 400 °C, the R_s behaviour can be best described by the Pippard model, indicating an excellent quality of the single-domain

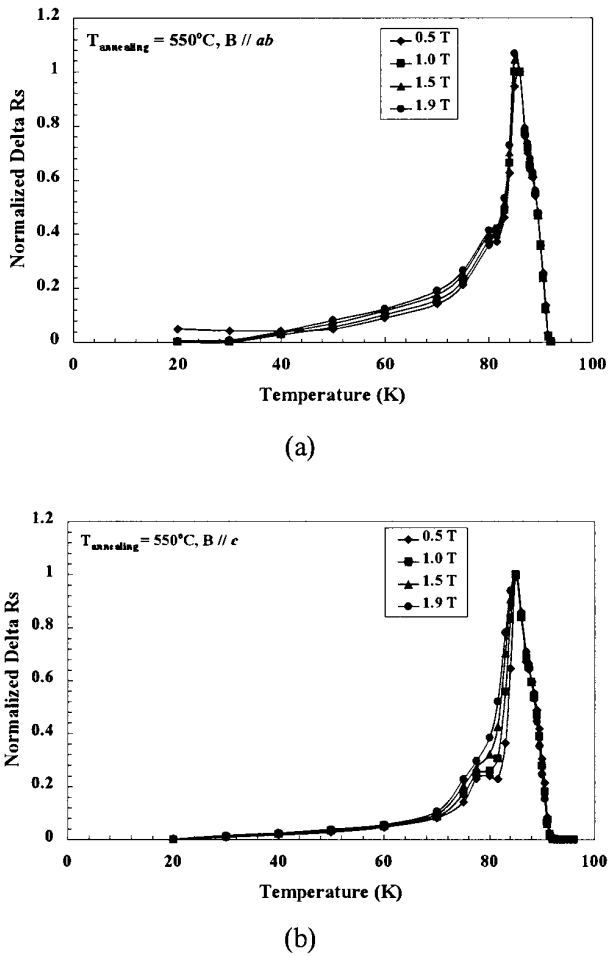

Figure 8. Normalized ΔR_s versus temperature for the sample annealed at 550 °C: (a) the fields are parallel to the *ab*-plane, (b) the fields are parallel to the *c*-axis.

YBCO. As the oxygen structural disorders are introduced to the sample, however, the Pippard scaling breaks down, suggesting a new physical mechanism that may govern the rf losses.

Acknowledgments

This work was supported by a grant from the National Science Foundation under contract number ECS-9802281. HAB thanks the US Department of Energy (MISCON) for their financial support of this work (contract No. DE-FG02-90ER45427), and D B Pulling for technical assistance.

References

[1] Dubourdieu C, Senateur J P, Thomas O, Weiss F, Hensen S and Muller G 1998 Correlation between the microwave surface resistance and the volumic fraction of *a*-axis grains in YBaCuO films $YBa_2Cu_3O_{7-x}$ *Physica* C **308** 16–20

[2] Velichko A V, Cherpak N T, Izhyk E V, Kirichenko A Ya and Moroz A V 1998 Microwave power dependent surface resistance of $YBa_2Cu_3O_x$ superconductors: material quality linkage *Supercond. Sci. Technol.* **11** 716–29

[3] Buznikov N A and Pukhov A A 1998 The effect of non-superconducting defects on microwave breakdown of HTSC films *Supercond. Sci. Technol.* **11** 1201–8

[4] Qu D, Shi D, Lu S-L, Ferendeci A M and Mast D 1999 Net-shape processing of single-domain $YBa_2Cu_3O_x$ for a novel high-*Q* millimeter wave resonator *Physica* C **315** 36–44

[5] Qu D, Tent B A, Shi D, Lu S-L, Ferendeci A M and Mast D 1998 Effect of oxygen on RF properties in a single domain YBCO cavity resonator for microwave applications *IEEE ASB-98 Proc.*

[6] Shi D, Lahiri K, Qu D and Sagar S 1997 Surface nucleation, domain growth mechanisms, and factors dominating superconducting properties in seeded melt grown $YBa_2Cu_3O_x$ *J. Mater. Res.* **12** 3036–45

[7] Shi D, Qu D and Sagar S 1997 Domain-orientation dependence of levitation force in seeded melt grown single-domain $YBa_2Cu_3O_x$ *Appl. Phys. Lett.* **70** 3606–8

[8] Shi D, Qu D and Tent B 1998 Growth anisotropy in seeded melt growth of $YBa_2Cu_3O_x$ *Mater. Sci. Eng.* B **53** 18–22

[9] Jorgensen J D, Beno M A, Hinks D G, Soderholm L, Volin K L, Hitterman R L, Grace J D and Schuller I K 1987 *Phys. Rev.* B **36** 3608

[10] Jorgensen J D, Veal B W, Kwok W K, Crabtree G W, Umezawa A, Nowicki L J and Paulikas A P 1987 *Phys. Rev.* B **36** 5731

[11] Jorgensen J D, Veal B W, Paulikas A P, Nowicki L J, Crabtree G W, Claus H and Kwok W K 1990 *Phys. Rev.* B **41** 1863

[12] Kwok W K, Crabtree G W, Umezawa A, Veal B W, Jorgensen J D, Malik S K, Nowicki L J, Paulikas A P and Nunez L 1988 *Phys. Rev.* B **37** 106

[13] Jorgensen J D, Shaked H, Hinks D G, Dabrowski B, Veal B W, Paulikas A P, Nowicki L J, Crabtree G W, Kwok W K and Nunez L 1988 *Physica* C **153–155** 578

[14] Gordon J P 1961 *Rev. Sci. Instrum.* **32** 658

[15] Van Duzer T and Turner C W 1981 *Principles of Superconductive Devices and Circuits* (New York: Elsevier) p 130